

Parallel-coupled dual racetrack silicon micro-resonators for quadrature amplitude modulation

Ryan A. Integlia,¹ Lianghong Yin,¹ Duo Ding,³ David Z. Pan,³ Douglas M. Gill,⁴
and Wei Jiang^{1,2,*}

¹Department of Electrical and Computer Engineering, Rutgers University, Piscataway, NJ 08854, USA

²Institute for Advanced Materials, Devices, and Nanotechnology, Rutgers University, Piscataway, NJ 08854, USA

³Department of Electrical and Computer Engineering, University of Texas at Austin,
Austin, TX 78712, USA

⁴Alcatel-Lucent Bell Labs, 600 Mountain Avenue, Murray Hill, NJ 07974, USA

*wjiangnj@rci.rutgers.edu

Abstract: A parallel-coupled dual racetrack silicon micro-resonator structure is proposed and analyzed for M -ary quadrature amplitude modulation. The over-coupled, critically coupled, and under-coupled scenarios are systematically studied. Simulations indicate that only the over-coupled structures can generate arbitrary M -ary quadrature signals. Analytic study shows that the large dynamic range of amplitude and phase of a modulated over-coupled structure stems from the strong cross-coupling between two resonators, which can be understood through a delicate balance between the direct sum and the “interaction” terms. Potential asymmetries in the coupling constants and quality factors of the resonators are systematically studied. Compensations for these asymmetries by phase adjustment are shown feasible.

© 2011 Optical Society of America

OCIS Codes: (230.5750) Resonators; (230.4110) Modulators; (130.3120) Integrated optics devices.

References and Links

1. P. J. Winzer and R. J. Essiambre, “Advanced optical modulation formats,” *Proc. IEEE* **94**(5), 952–985 (2006).
2. G. P. Agrawal, *Fiber-Optic Communication Systems* (John Wiley & Sons, New York, 1997).
3. R. Soref, “The past, present, and future of silicon photonics,” *IEEE J. Sel. Top. Quantum Electron.* **12**(6), 1678–1687 (2006).
4. B. Jalali and S. Fathpour, “Silicon photonics,” *J. Lightwave Technol.* **24**(12), 4600–4615 (2006).
5. A. S. Liu, R. Jones, L. Liao, D. Samara-Rubio, D. Rubin, O. Cohen, R. Nicolaescu, and M. Paniccia, “A high-speed silicon optical modulator based on a metal-oxide-semiconductor capacitor,” *Nature* **427**(6975), 615–618 (2004).
6. Q. F. Xu, B. Schmidt, S. Pradhan, and M. Lipson, “Micrometre-scale silicon electro-optic modulator,” *Nature* **435**(7040), 325–327 (2005).
7. C. Li, L. J. Zhou, and A. W. Poon, “Silicon microring carrier-injection-based modulators/switches with tunable extinction ratios and OR-logic switching by using waveguide cross-coupling,” *Opt. Express* **15**(8), 5069–5076 (2007).
8. Y. C. Li, L. Zhang, M. P. Song, B. Zhang, J. Y. Yang, R. G. Beausoleil, A. E. Willner, and P. D. Dapkus, “Coupled-ring-resonator-based silicon modulator for enhanced performance,” *Opt. Express* **16**(17), 13342–13348 (2008).
9. D. M. Gill, M. Rasras, K. Y. Tu, Y. K. Chen, A. E. White, S. S. Patel, D. Carothers, A. Pomerene, R. Kamocsai, C. Hill, and J. Beattie, “Internal Bandwidth Equalization in a CMOS-Compatible Si-Ring Modulator,” *IEEE Photon. Technol. Lett.* **21**(4), 200–202 (2009).
10. D. M. Gill, S. S. Patel, M. Rasras, K. Y. Tu, A. E. White, Y. K. Chen, A. Pomerene, D. Carothers, R. L. Kamocsai, C. M. Hill, and J. Beattie, “CMOS-Compatible Si-Ring-Assisted Mach-Zehnder Interferometer With Internal Bandwidth Equalization,” *IEEE J. Sel. Top. Quantum Electron.* **16**(1), 45–52 (2010).
11. L. Zhang, J. Y. Yang, M. Song, Y. Li, B. Zhang, R. G. Beausoleil, and A. E. Willner, “Microring-based modulation and demodulation of DPSK signal,” *Opt. Express* **15**(18), 11564–11569 (2007).
12. L. Zhang, J. Y. Yang, Y. C. Li, M. P. Song, R. G. Beausoleil, and A. E. Willner, “Monolithic modulator and demodulator of differential quadrature phase-shift keying signals based on silicon microrings,” *Opt. Lett.* **33**(13), 1428–1430 (2008).

13. W. M. J. Green, M. J. Rooks, L. Sekaric, and Y. A. Vlasov, "Optical modulation using anti-crossing between paired amplitude and phase resonators," *Opt. Express* **15**(25), 17264–17272 (2007).
14. W. D. Sacher and J. K. S. Poon, "Microring quadrature modulators," *Opt. Lett.* **34**(24), 3878–3880 (2009).
15. L. L. Gu, W. Jiang, X. N. Chen, L. Wang, and R. T. Chen, "High speed silicon photonic crystal waveguide modulator for low voltage operation," *Appl. Phys. Lett.* **90**(7), 071105 (2007).
16. X. N. Chen, Y. S. Chen, Y. Zhao, W. Jiang, and R. T. Chen, "Capacitor-embedded 0.54 pJ/bit silicon-slot photonic crystal waveguide modulator," *Opt. Lett.* **34**(5), 602–604 (2009).
17. R. A. Soref and B. R. Bennett, "Electrooptical Effects in Silicon," *IEEE J. Quantum Electron.* **23**(1), 123–129 (1987).
18. V. A. Mashkov and H. Temkin, "Propagation of eigenmodes and transfer amplitudes in optical waveguide structures," *IEEE J. Quantum Electron.* **34**(10), 2036–2047 (1998).
19. A. Hardy and W. Streifer, "Coupled modes of multiwaveguide systems and phased arrays," *J. Lightwave Technol.* **4**(1), 90–99 (1986).
20. C.-M. Kim and Y.-J. Im, "Switching operations of three-waveguide optical switches," *IEEE J. Sel. Top. Quantum Electron.* **6**(1), 170–174 (2000).
21. W. Jiang and R. T. Chen, "Multichannel optical add-drop processes in symmetrical waveguide-resonator systems," *Phys. Rev. Lett.* **91**(21), 213901 (2003).
22. A. Yariv, "Critical coupling and its control in optical waveguide-ring resonator systems," *IEEE Photon. Technol. Lett.* **14**(4), 483–485 (2002).
23. M. Soltani, S. Yegnanarayanan, Q. Li, and A. Adibi, "Systematic Engineering of Waveguide-Resonator Coupling for Silicon Microring/Microdisk/Racetrack Resonators: Theory and Experiment," *IEEE J. Quantum Electron.* **46**(8), 1158–1169 (2010).
24. M. H. Khan, H. Shen, Y. Xuan, L. Zhao, S. J. Xiao, D. E. Leaird, A. M. Weiner, and M. H. Qi, "Ultrabroad-bandwidth arbitrary radiofrequency waveform generation with a silicon photonic chip-based spectral shaper," *Nat. Photonics* **4**(2), 117–122 (2010).
25. W. A. Zortman, D. C. Trotter, and M. R. Watts, "Silicon photonics manufacturing," *Opt. Express* **18**(23), 23598–23607 (2010).
26. B. Razavi, *Principles of Data Conversion System Design* (Wiley-IEEE Press, Piscataway, NJ, 1994).
27. N. H. E. Weste and D. M. Harris, *CMOS VLSI Design: A Circuit and Systems Perspective* (Addison-Wesley, Upper Saddle River, NJ, 2010).
28. W. Jiang, L. Gu, X. Chen, and R. T. Chen, "Photonic crystal waveguide modulators for silicon photonics: Device physics and some recent progress," *Solid-State Electron.* **51**(10), 1278–1286 (2007).
29. D. A. B. Miller, "Device Requirements for Optical Interconnects to Silicon Chips," *Proc. IEEE* **97**(7), 1166–1185 (2009).

1. Introduction

Advanced optical modulation formats could offer significant advantages for optical communications [1,2]. For example, quadrature phase-shift keying provides higher spectral efficiency, better tolerance to fiber nonlinearity and chromatic dispersion, and enhanced receiver sensitivity compared to on-off keying. Traditional lithium niobate (LiNbO₃) modulators can be used for such modulation. However, LiNbO₃ modulators are relatively large in size. For a general M -ary modulation format that requires a large number of optical modulator components along with their driving signal circuitries, the overall size of the entire modulator is rather cumbersome. Recent breakthroughs in silicon photonics [3,4], particularly silicon based optical modulators [5,6], have fundamentally changed the landscape of modulator technology. Notably, micro-resonator based silicon modulators [6–10] constitute an ideal candidate for optical modulation due to their compact size, low power consumption, and ease of monolithic integration with driving circuitries on the same silicon chip. Most research on silicon microring modulators employed intensity modulation in binary formats. Recently, microring resonator based modulators for differential binary phase-shift-keying and differential quadrature phase-shift keying (QPSK) have been proposed, and satisfactory performances have been predicted [11,12]. Another work employed the anti-crossing between paired amplitude and phase resonators and demonstrated enhanced sensitivity to the input drive signal [13]. A high- Q microring quadrature modulator incorporating dual 2×2 Mach-Zehnder interferometers has also been recently proposed with beneficial performance [14].

We propose a novel parallel-coupled dual racetrack micro-resonator structure, illustrated in Fig. 1(a), for phase-shift keying and M -ary quadrature amplitude modulation (QAM). Two identical racetrack resonators are symmetrically side-coupled in parallel to a through waveguide in the center. The modulator can be fabricated on a silicon-on-insulator (SOI)

wafer. The carriers can be injected or depleted from the racetrack resonators using a *pin* diode [15] or metal-oxide-semiconductor capacitor [16] embedded in a silicon waveguide. The plasma dispersion effect [17] of the injected carriers causes a change of refractive index, Δn_1 , Δn_3 , in each racetrack resonator, which modifies the cross-coupled resonances of the two racetrack resonators. By carefully choosing the voltage signals applied to each resonator, the amplitude and phase of output optical signal can be controlled to generate arbitrary M -ary quadrature signals.

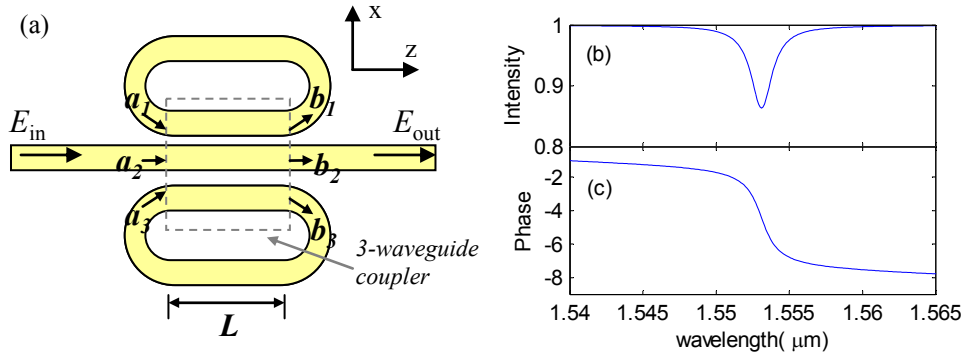


Fig. 1. Parallel-coupled dual racetrack resonators. (a) schematic of the structure, and typical spectra for an over-coupled structure: (b) output intensity and (c) phase in radians.

A distinctive feature of the proposed structure is that the coherent cross-coupling between the two racetrack resonators mediated by the center waveguide drastically modifies the amplitude/phase characteristics of resonance. This enables M -ary quadrature signal generations including quadrature phase shift keying (QPSK). The outcome of the cross-coupling of the resonances is fairly complex. However, our analysis shows that it can be understood through the direct sum and coherent “interaction” of the optical characteristics of two individual resonators as presented in Sec. 2.4. The structure of this paper is organized as follows. First the cross-coupling between the racetrack resonators is analyzed and the output transfer function of the proposed structure is presented. The critical coupling condition is obtained. Systematic studies of the over-coupled, critically coupled, and under-coupled scenarios for the parallel-coupled racetrack resonator structure indicate that strong over-coupling case is desired for arbitrary M -ary quadrature signal generation. The interaction between the resonances of two racetracks is analyzed, and its critical role in M -ary quadrature signal generation is presented. The effects of asymmetries in the coupling strengths and quality factors of resonators are systematically studied, and phase compensations for such asymmetries are presented. Lastly, the electrical aspects of the proposed modulators are briefly discussed, followed by a conclusion.

2. Principles of parallel-coupled racetrack resonators

2.1 Cross-coupling analysis and output transfer function

The coupling between the two racetrack resonators and the through-waveguide in Fig. 1(a) can be described by multi-waveguide coupling theory [18–20]. Assume the fields in three identical single-mode waveguides have slowly varying envelopes $u_n(z)$

$$\mathbf{E}_n(x, y, z) = \mathbf{M}_n(x, y) \exp(i\beta z) u_n(z), \quad n = 1, 2, 3, \quad (1)$$

where $\mathbf{M}_n(x, y)$ is the lateral mode profile, β is the propagation constant along the waveguide axis z for an isolated waveguide. For the parallel coupled racetrack resonator structure in Fig. 1, the input fields and output fields of the coupling segments are given by

$$\begin{aligned}\mathbf{E}_n^{(in)}(x, y, 0) &= \mathbf{M}_n(x, y)u_n(0) \equiv \mathbf{M}_n(x, y)a_n, \\ \mathbf{E}_n^{(out)}(x, y, L) &= \mathbf{M}_n(x, y)\exp(i\beta L)u_n(L) \equiv \mathbf{M}_n(x, y)b_n,\end{aligned}\quad (2)$$

where a_n and b_n are the normalized input and output complex amplitudes, respectively. The solution of the coupled mode equations yields [20]

$$\begin{bmatrix} b_1 \\ b_2 \\ b_3 \end{bmatrix} = \exp(i\beta L) \begin{bmatrix} c_1 + 1/2 & c_2 & c_1 - 1/2 \\ c_2 & 2c_1 & c_2 \\ c_1 - 1/2 & c_2 & c_1 + 1/2 \end{bmatrix} \begin{bmatrix} a_1 \\ a_2 \\ a_3 \end{bmatrix}, \quad (3)$$

where

$$c_1 = \frac{1}{2} \cos(\sqrt{2}\kappa L), \quad c_2 = \frac{1}{\sqrt{2}} i \sin(\sqrt{2}\kappa L).$$

The strength of the cross-coupling between the two racetrack resonators mediated by the through waveguide is given by $|c_1 - 1/2|$. In addition, light propagation along a racetrack gives rise to the following relations

$$\begin{aligned}a_1 &= \eta_1 \exp(i\theta_1)b_1, \\ a_3 &= \eta_3 \exp(i\theta_3)b_3,\end{aligned}\quad (4)$$

where the amplitude attenuation along a racetrack is given by $\eta_n < 1$, and the phase shift is given by θ_n . Assuming a unity input amplitude $a_2 = 1$, the output amplitude b_2 can be solved from Eqs. (3) and (4)

$$E_{out} = b_2 = \frac{e^{i\phi} \left[-(1/2 - c_1)(\Delta u_1 + \Delta u_3) + 2c_1 \Delta u_1 \Delta u_3 \right]}{(1/2 - c_1)(\Delta u_1 + \Delta u_3) + \Delta u_1 \Delta u_3}, \quad (5)$$

where $\phi = \beta L$, and

$$\Delta u_n \equiv \frac{1}{e^{i\phi + i\theta_n} \eta_n} - 1, \quad n = 1, 3, \quad (6)$$

Because of the symmetry of the structure shown in Fig. 1(a), the output amplitude, Eq. (5), only involves terms symmetric with respect to an interchange of Δu_1 and Δu_3 . As such, the symmetry of the structure can be utilized to help simplify the understanding of the device principles, as noted in the study of other devices [21]. Detailed analysis of a modulated symmetric dual racetrack resonator structure will be given in the following sections.

2.2 Critical coupling condition and vanishing amplitude for a modulated over-coupled structure

The critical coupling condition [22] can be obtained by setting $b_2 = 0$ in Eq. (5). For symmetric parallel-coupled racetracks without modulation ($\Delta u_1 = \Delta u_3$), one readily shows that the critical coupling condition for such a parallel-coupled dual racetrack structure is given by

$$\eta_1 = 2c_1 = \cos \sqrt{2}\kappa L. \quad (7)$$

The asymmetric cases will be discussed in a later section.

For modulated racetracks, the phase shift θ_n in each ring will be a linear function of the refractive index changes, Δn_n , due to carrier injection or depletion in the respective racetrack resonator. Therefore the output amplitude b_2 depends on Δn_n through the phase shift terms. To understand the modulation characteristics, it is helpful to rewrite the output amplitude in the following form

$$b_2 = e^{i\varphi} \left[-1 + \frac{(2c_1 + 1)}{(1/2 - c_1)(1/\Delta u_1 + 1/\Delta u_3) + 1} \right]. \quad (8)$$

As c_1 is a real number, for a modulated symmetric ($\eta_1 = \eta_3$) dual-racetrack structure, the output amplitude can vanish only if $\Delta u_1 = \Delta u_3^*$. Indeed, one can show that even if the critical coupling condition is not satisfied in absence of modulation, the *modulated* amplitude can still vanish under the following modulation condition

$$\varphi + \theta_1 = 2m_1\pi - \Delta\theta, \text{ and } \varphi + \theta_3 = 2m_3\pi + \Delta\theta, \quad (9a)$$

$$\cos \Delta\theta = \eta_1 \left[1 + \frac{c_1(1/\eta_1^2 - 1)}{c_1 + 1/2} \right], \quad (9b)$$

where m_1 and m_3 are two integers. For real nonzero $\Delta\theta$, this requires

$$\eta_1 > 2c_1 = \cos \sqrt{2}\kappa L, \quad (10)$$

which corresponds to over-coupling in comparison to Eq. (8). The spectra of an over-coupled dual racetrack structure (without modulation) are illustrated in Fig. 1(b) and (c).

2.3 Arbitrary M-ary quadrature signal generation capability

For intensity and phase modulation, the refractive index of the silicon waveguides in each racetrack is varied on the order of 0.001. Such an amount of Δn can be achieved with carrier concentration changes $\Delta N_e, \Delta N_h \sim 3 \times 10^{17} \text{cm}^{-3}$ according to the well-known plasma dispersion relation reported in [17].

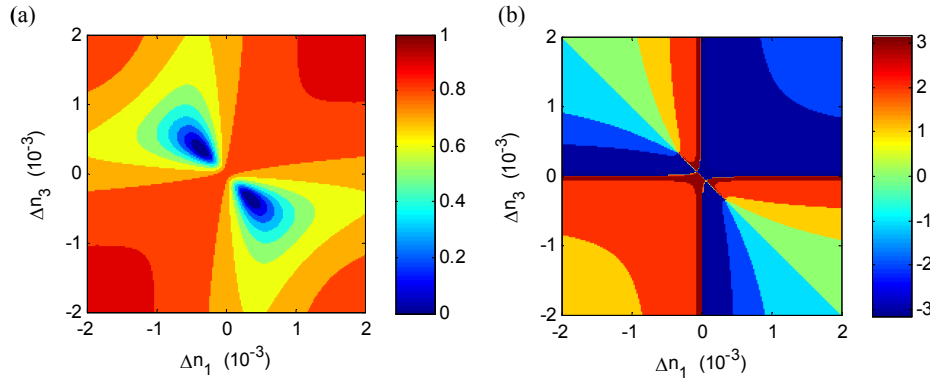


Fig. 2. Intensity (a) and phase (b) variations under refractive index modulation for the parallel-coupled dual racetrack resonators. $r_1 = r_3 = 3\mu\text{m}$, $L = 3\mu\text{m}$, $\eta_1 = \eta_3 = 0.994$, $c_1 = 0.4243$. The intensity vanishes at two points $(\Delta n_1, \Delta n_3) = (\pm 3.5 \times 10^{-4}, \mp 3.5 \times 10^{-4})$. The color code for the phase is in radians in (b).

Figure 2 depicts the simulated intensity and phase variations as a function of refractive index variations Δn_1 and Δn_3 at the resonant wavelength for an over-coupled structure. The structure parameters are $r_1 = r_3 = 3\mu\text{m}$, $L = 3\mu\text{m}$, $\eta_1 = \eta_3 = 0.994$, $c_1 = 0.4243$. Note that compact silicon racetrack resonators have been systematically characterized recently [23]. It was shown that the coupling strength and quality factor can be varied over large ranges by changing the Si pedestal layer thickness of the rib waveguide and modifying the gap width between the waveguide and the resonator. The parameters used here are in accordance with the ranges given Ref [23]. Evidently, the intensity vanishes at two points $(\Delta n_1, \Delta n_3) = (\pm 3.5 \times$

10^{-4} , $\mp 3.5 \times 10^{-4}$), in accordance with the analytic results given in Eq. (9)b). In all phase plots starting from Fig. 2, the overall constant phase factor $e^{i\phi}$ in b_2 is omitted to better illustrate the symmetry of the modulated output. On a side note, if η_1 and η_3 decrease simultaneously ($\eta_1 = \eta_3$), the two “eyes” on the diagonal of Fig. 2(a) widen and the phase contours in Fig. 2(b) expand accordingly.

To visualize the complex amplitude, $E_{\text{out}}(\Delta n_1, \Delta n_3)$, for M -ary signal generations, the ensemble of complex b_2 values for all values of Δn_1 and Δn_3 are mapped onto the complex plane of the normalized output electric field. Each blue point in Fig. 3(a) gives the amplitude and phase of the output signal for a particular pair of Δn_1 , Δn_3 values in the aforementioned range. Evidently, the ensemble of blue points covers most part of the unit circle (the symbol space), therefore, allowing for the access of a wide range of amplitude and phase values. A close examination of Fig. 2 indicates that the intensity and phase varies widely in the second and fourth quadrants where Δn_1 and Δn_3 have opposite signs, which corresponds to a push-pull configuration. In contrast, the intensity and phase are much less sensitive to Δn_1 and Δn_3 when they have the same sign. Indeed, our simulations indicate that the push-pull configuration is usually responsible for over 80% of coverage on the complex E plane. Hence a push-pull modulation configuration is preferred for such a parallel-coupled dual-racetrack structure.

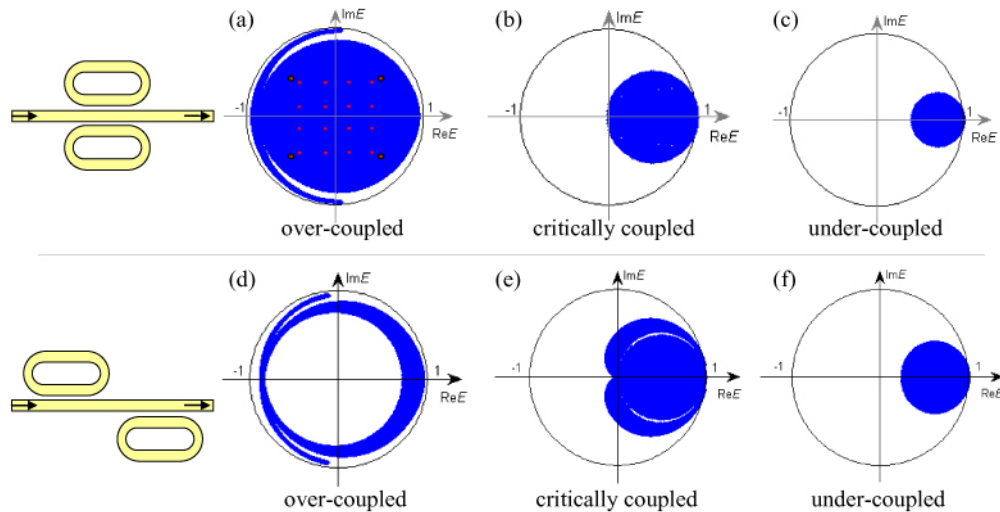


Fig. 3. Mapping of the normalized complex output field amplitude E_{out} on the complex plane for refractive index Δn_1 , Δn_3 varying in the range of $-0.002 \sim 0.002$. (a)-(c) for parallel-coupled dual racetrack resonators; (d)-(f) for two uncoupled racetrack resonators in series. Evidently, only case (a) is suitable for arbitrary M -ary quadrature signal generation. Constellations for QPSK (brown circles) and 16-QAM (red squares) modulation formats are illustrated in (a).

2.4 The cross-coupling of two racetrack resonances: direct sum and “interaction”

It should be noted that the broad coverage inside the unit circle observed in Fig. 3(a) is a signature of the *strong cross-coupling* between the two racetrack resonators mediated by the center waveguide. To illustrate this point, the simulated typical coverage of a critically coupled case and an under-coupled case is shown in Fig. 3(b) and (c), respectively, for parallel-coupled dual racetrack resonators. In addition, the simulated typical coverage for two *uncoupled* racetrack resonator in series is plotted in Fig. 3(d)-(f). None of the cases illustrated in Fig. 3(b)-(f) has adequate coverage for arbitrary M -ary quadrature signal generation.

The cross-coupling present in the parallel coupled racetrack resonators helps only the over-coupling case to achieve sufficient coverage over all four quadrants inside the unit circle. It can be shown that such a behavior stems from a delicate balance between the direct sum

term $\Delta u_1 + \Delta u_3$ and the “interaction” term $\Delta u_1 \Delta u_3$ on both the numerator and denominator in Eq. (5). Based on their definitions $\Delta u_n = (1 - e^{i\varphi+i\theta_n} \eta_n) / e^{i\varphi+i\theta_n} \eta_n$, Δu_n can be regarded as the *normalized* change of the field amplitude after one round-trip propagation in a racetrack. Here the initial field amplitude is unity, and the amplitude change is *normalized by the final field* amplitude $e^{i\varphi+i\theta_n} \eta_n$. For a racetrack without modulation ($\Delta n_1 = \Delta n_3 = 0$), Δu_i is small (on the order of $1 - \eta_1$) near resonance, and Δu_1 and Δu_3 are in phase. Therefore, we find

$$|\Delta u_1 \Delta u_3| \ll |(1/2 - c_1)(\Delta u_1 + \Delta u_3)|$$

because $1 - \eta_1 < 2(1/2 - c_1)$ according to the strong coupling condition. The dominance of the direct sum term in Eq. (5) yields an output amplitude close to -1 . With sufficient modulation in a push-pull configuration, Δu_n can gain large imaginary parts ($\text{Im}(\Delta u_n) \sim \Delta \theta_n$, up to ± 0.09 at $\Delta n_n = 0.001$) with opposite signs whereas their real parts remain small. Therefore, the product term exceeds the sum by a large margin, $|\Delta u_1 \Delta u_3| \gg |\Delta u_1 + \Delta u_3|$ such that $(1/2 - c_1)(\Delta u_1 + \Delta u_3)$ and $\Delta u_1 \Delta u_3$ in Eq. (5) become comparable. Now the output amplitude can take virtually any value. Particularly, the two terms in the numerator can exactly cancel each other so that the output amplitude vanishes. Hence the large dynamic range of $|(1/2 - c_1)(\Delta u_1 + \Delta u_3) / \Delta u_1 \Delta u_3|$ in the over-coupling case causes the output amplitude given by Eq. (5) to vary widely, traversing a large fraction of the area in the unit circle. Thus the output amplitude and phase have a large dynamic range. In contrast, for an under-coupling case, it is straightforward to show that, in general,

$$|(1/2 - c_1)(\Delta u_1 + \Delta u_3)| < |\Delta u_1 \Delta u_3|.$$

The dominance of the “interaction” term limits the accessible area in the unit circle.

3. Asymmetry effect in parallel-coupled dual racetrack resonators

As two racetrack resonators are involved in this structure, their asymmetry due to fabrication imperfections can be a major concern for practical applications. Note that the relatively long straight segments of racetracks ensure that the cross-coupling between the two resonators is insensitive to small misalignment between the left and right racetracks. As two racetracks can be patterned in one e-beam lithography process with a typical positioning accuracy of 20nm or better, the misalignment is estimated less than 1% for a coupling length $L > 2\mu\text{m}$. Optical path differences between the two racetracks can usually be compensated by a proper DC bias or by additional thermo-optic heaters [24,25]. However, the asymmetries in quality factors and coupling ratios cannot be directly compensated as easily. Therefore, their impacts on the device performance must be evaluated.

3.1 Asymmetric coupling

For three parallel waveguides with asymmetric coupling constants, the coupled mode equations can be written as

$$\frac{d}{dz} \begin{bmatrix} u_1(z) \\ u_2(z) \\ u_3(z) \end{bmatrix} = i \begin{bmatrix} 0 & \kappa_{12} & 0 \\ \kappa_{12} & 0 & \kappa_{23} \\ 0 & \kappa_{23} & 0 \end{bmatrix} \begin{bmatrix} u_1(z) \\ u_2(z) \\ u_3(z) \end{bmatrix}, \quad (11)$$

where the coupling constants between waveguide pairs (1,2) and (2,3) are κ_{12} and κ_{23} , respectively. To solve such a set of differential equation, $\frac{d}{dz}[u_m] = i[\kappa_{mn}][u_n]$, the coupling matrix is decomposed into the following form $[\kappa_{mn}] = X\Lambda X^+$, where Λ is a diagonal matrix

whose diagonal elements are the eigenvalues of the matrix $[\kappa_{mn}]$, the columns of X are the eigenvectors of $[\kappa_{mn}]$, and $XX^+ = I$. The original equation can then be integrated according to

$$[u_m(z)] = \exp(i[\kappa_{mn}]z)[u_n(0)] = X \exp(i\Lambda z)X^+[u_n(0)]. \quad (12)$$

Thus the solution of Eq. (11) is given by

$$\begin{bmatrix} u_1(z) \\ u_2(z) \\ u_3(z) \end{bmatrix} = \begin{bmatrix} \cos(\kappa_+ z)\rho_1^2 + \rho_3^2 & i \sin(\kappa_+ z)\rho_1 & \cos(\kappa_+ z)\rho_1\rho_3 - \rho_1\rho_3 \\ i \sin(\kappa_+ z)\rho_1 & \cos(\kappa_+ z) & i \sin(\kappa_+ z)\rho_3 \\ \cos(\kappa_+ z)\rho_1\rho_3 - \rho_1\rho_3 & i \sin(\kappa_+ z)\rho_3 & \cos(\kappa_+ z)\rho_3^2 + \rho_1^2 \end{bmatrix} \begin{bmatrix} u_1(0) \\ u_2(0) \\ u_3(0) \end{bmatrix}, \quad (13)$$

where $\kappa_+ = \sqrt{\kappa_{12}^2 + \kappa_{23}^2}$, $\rho_1 = \kappa_{12} / \kappa_+$, and $\rho_3 = \kappa_{23} / \kappa_+$. In a symmetric case, $\kappa_+ = \sqrt{2}\kappa_{12} = \sqrt{2}\kappa_{23} = \sqrt{2}\kappa$, $\rho_1 = \rho_3 = 1/\sqrt{2}$, Eq. (13) returns to Eq. (3). The output amplitude b_2 can be solved in a procedure similar to that given for the symmetric case. After lengthy calculations, the final result is surprisingly simple

$$b_2 = e^{i\varphi} \left[-1 + \frac{1 + \cos(\kappa_+ L)}{[1 - \cos(\kappa_+ L)](\rho_1^2 / \Delta u_1 + \rho_3^2 / \Delta u_3) + 1} \right], \quad (14)$$

where Δu_n are defined the same way as in the symmetric case. Comparing Eq. (14) and Eq. (8), it is evident that all asymmetry effects can be effectively factored into the term

$$\rho_1^2 / \Delta u_1 + \rho_3^2 / \Delta u_3 = \frac{\kappa_{12}^2}{\kappa_+^2} \frac{e^{i\varphi+i\theta_1} \eta_1}{1 - e^{i\varphi+i\theta_1} \eta_1} + \frac{\kappa_{23}^2}{\kappa_+^2} \frac{e^{i\varphi+i\theta_3} \eta_3}{1 - e^{i\varphi+i\theta_3} \eta_3}. \quad (15)$$

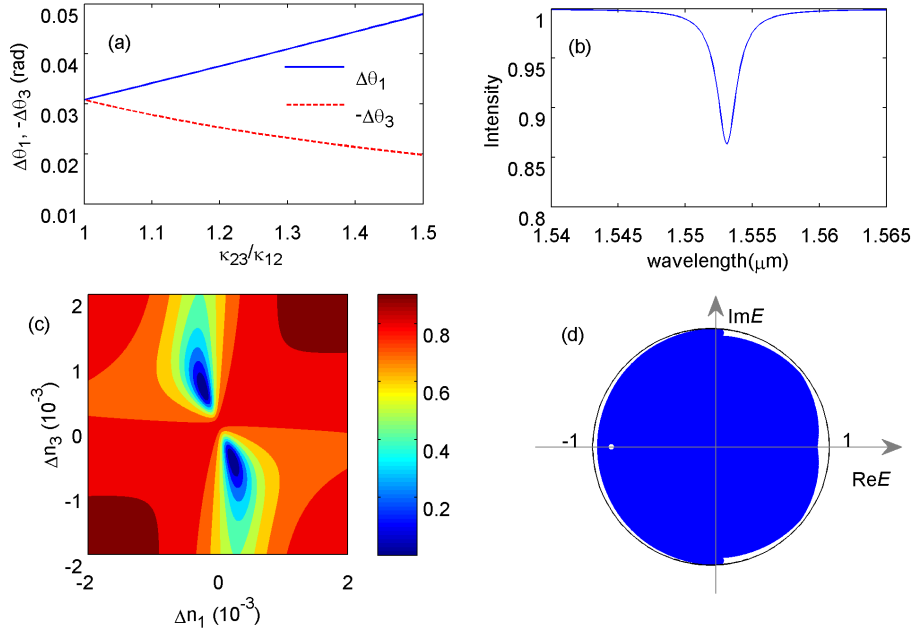


Fig. 4. Effect of asymmetric coupling constants. (a) Required phase compensation in each racetrack for up to 50% asymmetry in the coupling ratios. The characteristics of the asymmetric dual racetrack structure for the worst case scenario ($\kappa_{23}/\kappa_{12} = 1.5$) are illustrated in (b)-(d). (b) Output spectrum without modulation; (c) Intensity variation with index modulation; (d) Mapping of the output field on the complex plane. All parameters are the same as those used in Fig. 2 except κ_{23}/κ_{12} is varied.

As a consequence, for reasonable asymmetries in the coupling constants and resonator quality factors, there exists a pair of phases $\Delta\theta_1$ and $\Delta\theta_3$ such that the output amplitude b_2 vanishes. The required phase variations are plotted against the asymmetric coupling ratio, κ_{23}/κ_{12} , in Fig. 4(a) for up to 50% asymmetry. As $\Delta\theta_1$ and $\Delta\theta_3$ generally have opposite signs, we plot $\Delta\theta_1$ and $-\Delta\theta_3$ to better illustrate the deviation from symmetry. Note that $\Delta\theta_1 = -\Delta\theta_3$ is required for $b_2 = 0$ in a symmetric structure ($\kappa_{23}/\kappa_{12} = 1$), according to Eq. (9). The difference between $\Delta\theta_1$ and $-\Delta\theta_3$ becomes larger as the asymmetry increases.

Figure 4(a) shows that although it is not easy to directly compensate the asymmetric coupling constants themselves, asymmetric phase shifts (through different DC biases applied to the two resonators) can be introduced to recover the low intensity states ($b_2 \sim 0$). The unmodulated output spectrum for the worst case ($\kappa_{23}/\kappa_{12} = 1.5$) is illustrated in Fig. 4(b) and shows no anomaly. However, the intensity variation upon refractive index modulation shows obvious distortion from the symmetric case. Nonetheless, two features remain: (1) there are two points with relatively small index changes ($\pm 2.2 \times 10^{-4}$, $\mp 5.4 \times 10^{-4}$) where the intensity vanishes; (2) the intensity varies significantly in the push-pull configuration and much less otherwise. The coverage on the complex E plane is slightly enhanced, although a small hole exists at a large amplitude value, which may limit the maximum accessible amplitude to 0.78 for a generic M -ary modulation format.

3.2 Asymmetric quality factors

The effects of asymmetric quality factors are illustrated in Fig. 5. The required phase shifts, $\Delta\theta_1$ and $-\Delta\theta_3$, for vanishing b_2 , are plotted against the ratio of the quality factors in Fig. 5(a). The unloaded quality factor Q_1 is fixed at its original value $\sim 2.5 \times 10^4$.

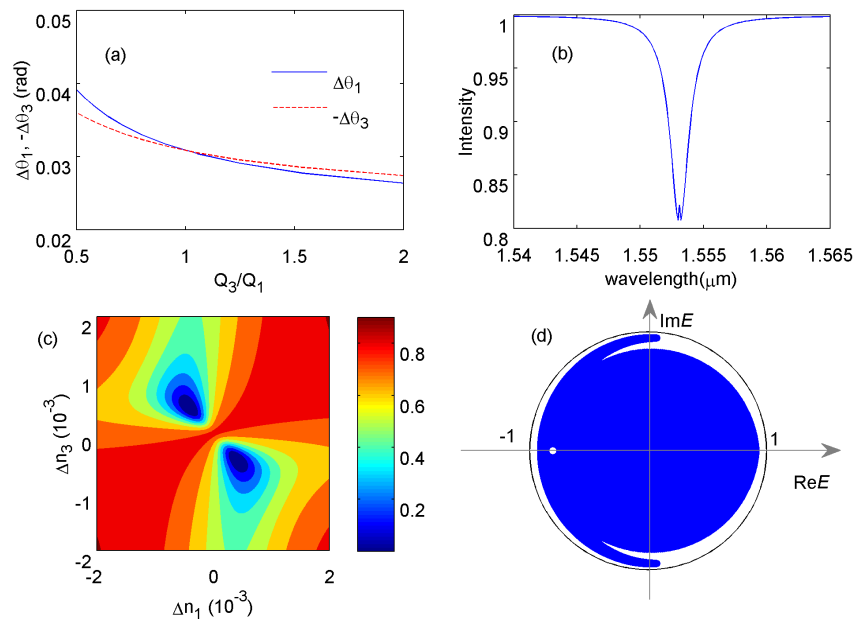


Fig. 5. Effect of asymmetric quality factors. (a) Required phase compensation in each racetrack for asymmetry in the quality factors. The characteristics of the asymmetric dual racetrack structure for the worst case scenario ($Q_3 = 0.5Q_1$) are illustrated in (b)-(d). (b) Output spectrum; (c) Intensity variation with index modulations; (d) Mapping of the output field on the complex plane. All parameters are the same as those used in Fig. 2 except η_3 is varied to yield different Q_3 .

Note that $\Delta\theta_1 = -\Delta\theta_3$ for the case of $Q_3/Q_1 = 1$ in accordance to the symmetric case. The un-modulated output spectrum for the worst case ($Q_3/Q_1 = 0.5$) is illustrated in Fig. 5(b). A small yet noticeable spike appears at the resonance due to the asymmetric quality factors of the two racetrack resonators. The modulated intensity variation upon refractive index modulation depicted in Fig. 5(c) shows less severe distortion compared to the distortion observed in the Fig. 4(c). Again, two features remain: (1) there are two points with relatively small index changes ($\pm 4.4 \times 10^{-4}$, $\mp 4.1 \times 10^{-4}$) where the intensity vanishes; (2) the intensity varies significantly in the push-pull configuration and much less otherwise. The coverage on the complex E plane slightly deteriorates. There exists a small hole, which may limit the maximum accessible amplitude to 0.74 for a generic M -ary modulation format.

Note that the evolution from symmetry to the worst case asymmetry is gradual. For example, the two “eyes” in Fig. 4(c) gradually narrow as the asymmetry in the coupling constant worsens. Also, the centers of the “eyes” rotate clockwise around the origin ($\Delta n_1 = \Delta n_3 = 0$). As the asymmetry in the quality factors worsens, the “eye” centers do not narrow or rotate substantially although there are some deformations.

Overall, the asymmetry analysis presented above show that substantial asymmetries in coupling constants and quality factors of the two racetrack resonators can be compensated by refractive index changes on the order of 4×10^{-4} , which can be readily provided with a low-power heater or a small change of the DC bias. Fundamentally, such compensations are possible because all these asymmetries enter the output amplitude, Eq. (14), through the term given in Eq. (15). For structures with asymmetric η 's or Q 's, asymmetric phase shifts can restore the value of the term given in Eq. (15) to a corresponding symmetric structure. Specifically, to achieve vanishing output intensity under modulation, a structure with 50% asymmetry in the coupling constant requires $(\Delta n_1, \Delta n_3) = (\pm 2.2 \times 10^{-4}, \mp 5.4 \times 10^{-4})$ whereas a symmetric structure requires $(\Delta n_1, \Delta n_3) = (\pm 3.5 \times 10^{-4}, \mp 3.5 \times 10^{-4})$. The difference between $|\Delta n_1|$ and $|\Delta n_3|$ in the asymmetric case is used to restore Eq. (15) to the value of the symmetric case such that $b_2 = 0$.

4. Discussion

In general, an encoder is needed to convert an original M -ary digital signal into the driving signal for the modulator. Consider the case of a QPSK signal with four symbols shown in Fig. 3(a). The encoder will have a two-bit input and two output ports. Each output port has four output voltage levels. The design of such an encoder and its supporting circuitries has been well studied in the state-of-the-art high-speed data conversion systems [26] and CMOS VLSI [27]. Under the given specifications (resolution, signal-to-noise ratio, bandwidth, driving power, etc.), this encoder can be easily architected and implemented as a high-speed digital-to-analog data converter, which can be fabricated economically using the silicon-on-insulator technology together with the dual racetrack resonator modulator. Note that a conventional nested Mach-Zehnder QPSK [1] modulator needs two output voltage levels for each port. The additional voltage levels required for the proposed QPSK modulator will somewhat increase the size of the driving circuitry. However, electronic devices such as transistors are generally significantly smaller than photonic devices. Therefore, the enlargement of the driving circuitry is usually negligible compared to the significant space saving offered by changing from a bulky nested Mach-Zehnder modulator to the proposed dual racetrack resonators.

Driving voltages and power consumption are important issues for silicon modulators used in optical interconnects [28,29]. For a nested Mach-Zehnder QPSK modulator which is biased across the minimum point of the transfer curve, a lower driving voltage and lower RF power consumption can be achieved at the expense of a lower maximum output intensity (which entails a trade-off with the detector sensitivity or the input laser power). For the proposed parallel-coupled dual racetrack modulator, a similar power reduction scheme is possible. For simplicity, we consider silicon racetrack resonators with embedded MOS capacitors, whose

index change is approximately linearly dependent on the voltage. As illustrated in Fig. 6(a), the driving power can be significantly lower at lower output intensity. Asymmetries of the coupling constants and quality factors could entail extra power penalty but the power remains reasonable. According to Fig. 6, if the asymmetry is large, electrical power penalty is significantly lower when the modulator operates at a lower output intensity level. Therefore, for a modulator that happens to have a large asymmetry due to imperfection in fabrication, the balance of the power trade-off may tip towards enhancing the detector sensitivity.

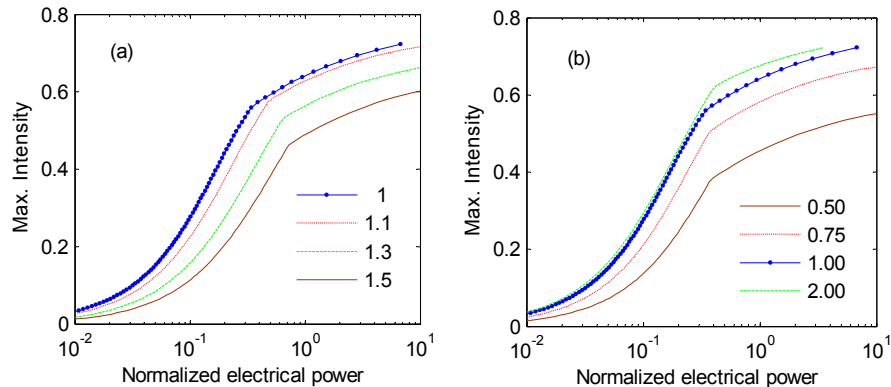


Fig. 6. Output intensity as a function of the driving power for parallel-coupled dual racetrack modulators with varying degrees of asymmetry. (a) For various κ_{23}/κ_{12} values and (b) For various Q_3/Q_1 values. The output intensity is normalized by the input intensity. The driving power is normalized by the power level corresponding to the case that each racetrack is driven to $\Delta n = 0.001$.

5. Conclusion

In summary, we have proposed and analyzed a parallel-coupled dual racetrack micro-resonator modulator for arbitrary M -ary quadrature signal generation. The critical coupling condition is obtained for such a structure. The intensity and phase modulations are obtained by varying the refractive indices of the silicon waveguides in the two parallel-coupled resonators. It is shown that a push-pull configuration effectively modulates the intensity and phase. The coverage of the complex plane of the output field E_{out} is systematically studied for over-coupling, critical-coupling, and under-coupling scenarios, and is compared to the corresponding scenarios of two uncoupled racetrack-resonators in series. It is found that only the over-coupling scenario of a parallel-coupled dual racetrack resonator structure results in adequate coverage for arbitrary M -ary quadrature signal generation. The interaction between the parallel-coupled racetrack resonators is key to the coverage of the complex E plane. In an over-coupled dual racetrack structure, a delicate balance is achieved between the direct sum and the interaction of the two racetrack resonances, which results in a large dynamic range of the output amplitude and phase. Particularly, the modulated intensity can reach zero in a push-pull configuration although the intensity of the un-modulated over-coupled racetrack resonators do not vanish at any wavelength. The effects of asymmetries in the coupling constants and quality factors are systematically studied. Despite the distortion of the intensity and phase mapping, small refractive index changes, which can be readily obtained with a reasonable thermal or electrical bias, can be used to compensate the asymmetry. The coverage of the complex E plane remains sufficient despite asymmetries.

Acknowledgments

The authors are grateful to Zhong Shi, Qianfan Xu, Lin Zhang, Rene-Jean Essiambre, and Ying Qian for helpful discussions. This work is supported in part by AFOSR Grants No. FA9550-10-C-0049 and No. FA9550-08-1-0394 (G. Pomrenke). R. A. I. acknowledges the partial support of a NSF IGERT Traineeship.